J Multidisciplinary Scientific Journal

MDPI

Article

Evaluation of Photodynamic Therapy Using AuNPs@Ce6 in 3D Cultures of Triple-Negative Breast Cancer

Aveline Ventura [1], Giulia Capizzani Gonçalves [1], Cristina Pacheco Soares [2], Luciana Barros Sant'anna [3], Vitor Luca Moura Marmo [1], Sônia Khouri Sibelino [1] and Leandro Raniero [1,*]

[1] Nanosensors Laboratory, Research & Development Institute, University of Vale do Paraíba, Av. Shishima Hifumi, 2911, Urbanova, São José dos Campos 12244-000, SP, Brazil; aveline.biomed@gmail.com (A.V.); giulia.engquimica@gmail.com (G.C.G.); vitorl.mmarmo@gmail.com (V.L.M.M.); skkhouri@gmail.com (S.K.S.)
[2] Dynamics of Cellular Compartments Laboratory, University of Vale do Paraíba, Av. Shishima Hifumi, 2911, Urbanova, São José dos Campos 12244-000, SP, Brazil; cpsoares@univap.br
[3] Histology and Regenerative Therapy Laboratory, University of Vale do Paraíba, Av. Shishima Hifumi, 2911, Urbanova, São José dos Campos 12244-000, SP, Brazil; lucianabsa@gmail.com
* Correspondence: lraniero@univap.br; Tel.: +55-12-3947-1132

Abstract

Conventional cancer treatments have limited efficacy for aggressive subtypes such as triple-negative breast cancer (TNBC), which points to the importance of new therapeutic strategies. Functionalized nanoparticles in conjunction with photodynamic therapy (PDT) represent a promising alternative. Additionally, 3D cell culture emerges as a more effective model, as it better replicates the structural and functional characteristics of the tumor microenvironment. In this study, 3D microtumors of TNBC were cultivated and treated with PDT using gold nanoparticles functionalized with Chlorin e6 (AuNPs@Ce6). Cell viability was assessed using the MTT colorimetric assay, combined with histological analysis using hematoxylin-eosin staining. The MTT assay and histological evaluation of the 3D spheroids demonstrated that PDT with AuNPs@Ce6 effectively reduced cell viability and induced necrotic morphological changes, while maintaining biocompatibility with the non-irradiated control group. These findings reinforce the potential of this approach for further investigation in TNBC models and underscore the value of 3D cultures as physiologically relevant and ethical alternatives to animal testing.

Keywords: 3D microtumors; PDT; gold nanoparticles; chlorin e6

Academic Editors: Mari Carmen Horrillo Güemes and Pietro Cipresso

Received: 22 September 2025
Revised: 28 October 2025
Accepted: 12 November 2025
Published: 17 November 2025

Citation: Ventura, A.; Gonçalves, G.C.; Soares, C.P.; Sant'anna, L.B.; Marmo, V.L.M.; Sibelino, S.K.; Raniero, L. Evaluation of Photodynamic Therapy Using AuNPs@Ce6 in 3D Cultures of Triple-Negative Breast Cancer. *J* **2025**, *8*, 43. https://doi.org/10.3390/j8040043

1. Introduction

The World Health Organization classifies cancer as a malignant tumor, which is characterized by disordered cell proliferation often associated with genetic mutations [1]. Breast cancer is one of the most common types diagnosed worldwide and stands out as the leading cause of cancer death among women [2]. Typically, it is asymptomatic in the early stages and is also present in various histopathological stages, thereby complicating early diagnosis. Conventional treatments include surgery, chemotherapy, radiotherapy, and hormone therapy, often used in combination according to the patient's clinical need [3]. However, these methods can compromise healthy cells by affecting the structure and function of tissues [4]. It is important to highlight that the triple-negative breast cancer (TNBC) subtype has the poorest prognosis among all breast cancers, characterized by high rates of recurrence and metastasis [5,6]. Moreover, TNBC lacks targeted therapeutic options,

as these tumors do not express estrogen, progesterone, or HER2 receptors, making systemic treatment largely dependent on chemotherapy [7].

In order to minimize side effects and increase overall survival, the study of new therapeutic methods has become a priority in the field of biomedical research, with emphasis on nanotechnology [8]. Researchers are developing nanoparticles functionalized with therapeutic agents, which have specific properties, for use in the diagnosis and treatment of cancers like breast cancer. This innovation allows for the selective targeting and administration of drugs to cancer cells, thereby reducing side effects and enhancing treatment effectiveness [9].

In parallel with the development of functionalized nanoparticles, photodynamic therapy (PDT) emerges as a promising technique to improve oncological treatments. This approach employs a photosensitizer (PS), which accumulates in tumor tissue and activates when exposed to light at a specific wavelength. This process produces reactive oxygen species, which selectively destroy cancer cells. In addition to directly eliminating the tumor, PDT can stimulate immune responses, enhancing cancer eradication [10].

Apart from that, much research has employed techniques such as in vitro cell culture to investigate the biological mechanisms involved in cancer treatment, enabling the analysis of cellular responses in a controlled laboratory environment. However, traditional two-dimensional (2D) cell culture models may not accurately reproduce the complex features of in vivo environments, hindering research. To overcome this limitation, three-dimensional (3D) culture has emerged as an effective alternative [11]. Three-dimensional cultures offer a more physiologically relevant environment, promoting enhanced interactions between cells and the extracellular matrix (ECM), which provides a more accurate representation of the in vivo environment. To the best of our knowledge, this study is among the first to quantitatively correlate the cytotoxic and histological effects of AuNPs@Ce6-mediated photodynamic therapy within long-term 3D spheroids of TNBC. The integration of quantitative cell viability assays with standard hematoxylin and eosin (H&E) staining enabled a complementary evaluation of microtumor structure and cellular damage. This approach provides new insights into the relationship between PDT-induced cytotoxicity and morphological alterations in physiologically relevant 3D tumor models, contributing to the preclinical understanding of nanostructure-mediated therapy.

2. Materials and Methods

2.1. Gold Nanoparticles Synthesis

Gold chloride trihydrate was dissolved in ultra-pure water (18.2 MΩ·cm) at 0.04% (*w*/*v*) and heated to ~98 °C under constant stirring at 1100 rpm. A 1% (*w*/*v*) sodium citrate solution was added to allow AuNPs nucleation by acting as a reducing and stabilizing agent [12]. The reaction was maintained at ~98 °C for 60 min to ensure complete reduction and stabilization of the nanoparticles. After cooling to room temperature, the colloidal suspension was stored at 4 °C in the dark. AuNP concentration was determined by UV–Vis spectroscopy using the Beer–Lambert law, assuming particles <85 nm in size and an extinction coefficient of 4.7×10^4 $M^{-1} \cdot cm^{-1}$ at the plasmon resonance peak [13].

2.2. Nanostructured Photosensitizer

The nanostructured photosensitizer (AuNPs@Ce6) is composed of gold nanoparticles conjugated with chlorin e6 (Ce6). For binding Ce6 on the AuNP surface, a thiol group was added to the Ce6 structure by coupling its carboxylic group with the amine group of cysteamine. This modification was performed by carbodiimide chemistry, forming a Ce6–cysteamine complex using the following molar ratio of reactants: 1 Ce6 (8.4 mM)/25 Sulfo NHS (187.5 mM)/10 EDC (83.5 mM)/3 Cysteamine (8 mM). The colloidal AuNPs

solution was incubated with the Ce6-cysteamine complex under constant agitation for 24 h. To purify the AuNPs@Ce6, the solution was centrifuged at 13,000 rpm for 5 min. After discarding the supernatant, ultrapure water was added to the precipitate [14].

The UV-visible spectra were collected by a DS-11 spectrophotometer (DeNovix DS-11, Wilmington, DE, USA). The hydrodynamic diameter and Zeta potential were measured using Zetasizer Nano ZS90 equipment (Malvern Instruments Limited, Worcestershire, UK) [15].

2.3. Two-Dimensional and 3D Cell Cultures

Monolayer cell cultures were established in 25 cm^2 flasks using complete L-15 medium (Leibovitz L4386, Sigma Life Science, Darmstadt, Germany) supplemented with 10% fetal bovine serum (FBS, 16000-044; Life Technologies Carlsbad, CA, USA). The human triple-negative breast cancer cell line MDA-MB-468, obtained from the Rio de Janeiro Cell Bank (BCRJ), was maintained at 37 °C in a humidified incubator (95% relative humidity) without additional CO_2. When the cultures reached confluence, the cells were detached with 0.025% trypsin-EDTA, centrifuged at 2000 rpm for 10 min, and resuspended in complete medium. Cell density was determined using a Neubauer chamber, and the final suspension was adjusted to 1×10^5 cells/mL for subsequent 3D spheroid formation [14].

The 3D cell culture was used to generate TNBC spheroids employing ultrapure agarose micromolds (3D Petri Dish®; MicroTissues, Inc., Sharon, MA, USA), as illustrated in Figure 1. Several microcavities were prepared in agarose gels (Ultrapure Agarose, Invitrogen, Carlsbad, CA, USA) by heating a sterile 2% agarose solution in 0.9% NaCl saline to 65 °C and pipetting it into sterile micromolds (Figure 1a). After solidification, the agarose molds were carefully removed, transferred to experimental plates, and exposed to UV light for 30 min for sterilization (Figure 1b). A cell suspension containing 1×10^5 cells/mL was then pipetted into the agarose molds, and multicellular spheroids gradually formed within the microcavities over an incubation period of approximately 40 days (Figure 1c).

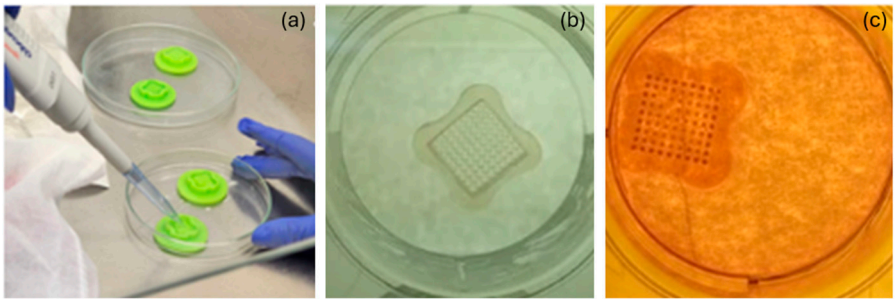

Figure 1. Spheroid cultivation process: (**a**) pipetting agarose into the molds; (**b**) molds containing only agarose without any cells added; (**c**) molds filled with culture medium that supports the development of spheroids.

2.4. Characterization of Spheroids by Confocal Fluorescence Microscope

For the structural analysis of the microtumors, the immunofluorescence technique for actin filaments was used. Initially, the spheroids were fixed with 4% paraformaldehyde for 15 min. After fixation, they were washed with cytoskeletal buffer (CSK), composed of 0.05 M NaCl, 0.15 M sucrose, 0.03 M $MgCl_2$, 0.05 M Tris base, and 0.5% Triton X-100 at a pH of 6.8 for 20 min, to allow cell permeabilization.

The samples were incubated with rhodamine-phalloidin (1:100 dilution) for 1 h and then contrasted with DAPI-containing mounting medium. Cytoskeletal structures and cell nuclei were analyzed, and images were captured using the ZEISS LSM 700 confocal fluorescence microscope (Carl Zeiss AG, Jena, Germany), with the Zeiss Plan-apochromat 63x/1.4 Oil Iris M27 objective.

2.5. Photodynamic Therapy and Cellular Mitochondrial Activity

Photodynamic therapy (PDT) experiments were performed using 3D cultures. The culture medium was replaced with the AuNPs@Ce6 suspension at 2 μg/mL, and the microtumors were incubated for 2 h. Subsequently, the microtumors were washed with PBS, and fresh complete culture medium was added before irradiation. Irradiation was carried out using an Irrad-Led5 660 LED system (Biopdi, São Carlos, São Paulo, Brazil) at a wavelength of 660 nm, a power density of 46.5 mW/cm^2, and an energy density of 39 J/cm^2, with the plate positioned 15 mm from the light source.

Three experimental groups were established under identical conditions: (a) untreated spheroids (control); (b) spheroids incubated with AuNPs@Ce6 and subsequently irradiated (PDT group); and (c) spheroids incubated with AuNPs@Ce6 but not irradiated (dark cytotoxicity control). For each condition, ten spheroids were transferred to individual wells of a 96-well plate containing 150 μL of culture medium. Each experiment was carried out in triplicate and repeated once independently to confirm reproducibility.

Cell viability was analyzed using the MTT colorimetric assay (3-(4,5-dimethylthiazol-2-yl)-2,5-diphenyltetrazolium bromide M5655; Sigma-Aldrich, Darmstadt, Germany), which quantifies cellular metabolic activity. Twenty hours after PDT application, 50 μL of MTT solution (2 mg/mL) were added to each well already containing 150 μL of culture medium, and the plates were incubated for 4 h at 37 °C under standard culture conditions. Subsequently, the medium was carefully removed and replaced with 200 μL of dimethyl sulfoxide (DMSO) to dissolve the formazan crystals. Absorbance was measured at 570 nm using a spectrophotometer, and the results were expressed as percentages relative to the absorbance of the control wells. Statistical differences among the groups were analyzed using one-way ANOVA followed by Tukey's post hoc test at a significance level of 0.05.

2.6. Histological Analysis of Cell Culture in 3D

After 40 days of culture, the samples were treated for 2 h with AuNPs@Ce6 and subsequently irradiated, followed by histological analysis to evaluate necrosis features within the spheroids. The microtumors were fixed in 4% paraformaldehyde for 72 h, then dehydrated and embedded in paraffin. For dehydration, two washes in absolute ethanol were performed, each consisting of three immersions of 4 s, ensuring complete removal of residual alcohol. Since paraffin is insoluble in water, the resulting paraffin blocks were sectioned into slices approximately 5 μm thick and mounted onto glass slides.

H&E staining was performed to visualize cellular structures, highlighting the cytoplasm and nuclei. The sections were washed in distilled water and immersed in Meyer's hematoxylin for 2 min, rinsed again in distilled water to remove excess dye, and then stained with eosin for 1 min. After staining, the slides were washed with distilled water, and excess moisture was removed using absorbent paper. Finally, coverslips were carefully placed over the sections, allowing the mounting medium to spread evenly and form a thin film between the slide and the coverslip. Once the medium stabilized, the coverslips adhered firmly, ensuring long-term preservation of the samples for microscopic analysis.

3. Results

Figure 2a shows the differences in the hydrodynamic diameter distribution between AuNPs@Ce6 (~36 nm) and unmodified AuNPs (~25 nm). Complementary TEM data for the bare nanoparticles were reported in reference [15]. Figure 2b presents the UV–Vis absorption spectra, highlighting the spectral profile of AuNPs@Ce6 in comparison to unbound Ce6 and bare AuNPs. The hydrodynamic size of the colloidal solution increased by approximately 11 nm, indicating the successful conjugation of Ce6 to the AuNPs, and an increase in negative Zeta potential magnitude (~−7 mV) indicates better colloidal stability

(Figure 2a). These results are further supported by Figure 2b, where the localized surface plasmon resonance (LSPR) of the gold nanoparticles exhibits a redshift, corresponding to the increase in particle size. Additionally, the absorption spectrum of AuNPs@Ce6 is a combination of the individual spectra of AuNPs and Ce6, with a shift that may be attributed to the influence of electronic density changes induced by the AuNPs [14,15]

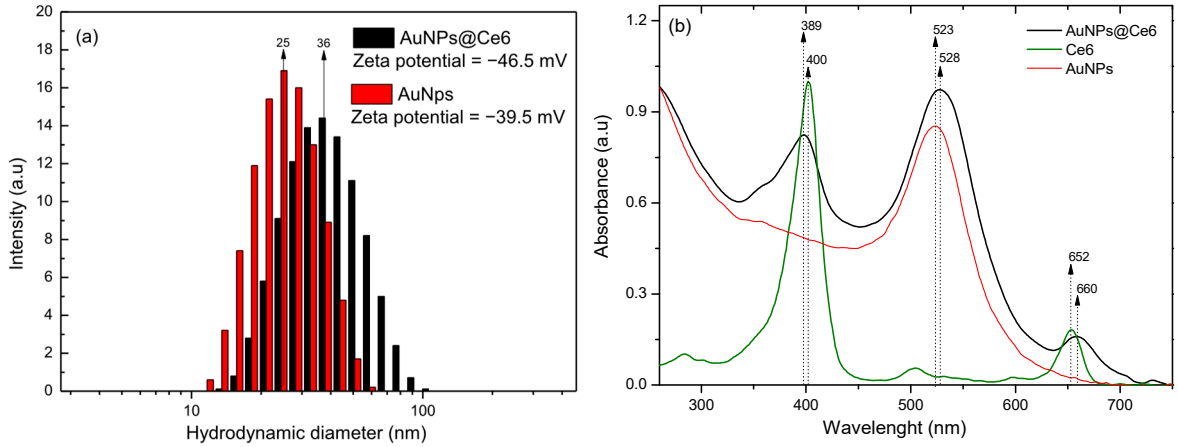

Figure 2. Characterization of AuNPs@Ce6: (**a**) hydrodynamic diameter distribution difference between AuNPs@Ce6 and AuNPs; (**b**) UV-visible spectrum of AuNPs@Ce6 compared to Ce6 and AuNps spectra.

Figure 3 shows the evolution of spheroid growth, parameterized by gelatin mold sizes (800 µm and 1400 µm). The percentage values represent the ratio of the cell-covered area to the unoccupied area. The red line indicates the linear fit, where the slope corresponds to the growth rate, calculated as the first derivative. The results reveal similar growth rates of 3.2 ± 0.2% and 3.9 ± 0.4% of the area covered per day for the 800 µm and 1400 µm mold diameters, respectively. For the smaller mold, spheroid growth initiates from the center and expands toward the gelatin border, whereas for the larger mold, cell growth progresses from the border toward the center. However, a period of 40 days is necessary to achieve a compact spheroid suitable for handling during experimental procedures.

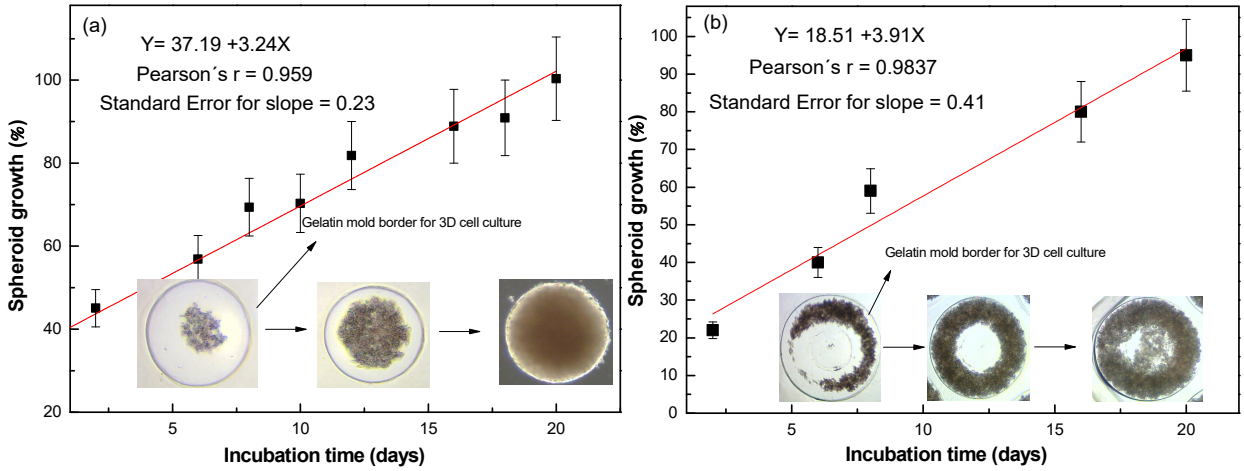

Figure 3. The evolution of spheroid growth parameterized by gelatin mold sizes: (**a**) 800 µm and (**b**) 1400 µm. The red line represents the linear fit, and the arrows indicate the growth progression.

Figure 4 shows the structural and morphological analysis of the microtumors after the culture period. The analysis was performed using immunofluorescence to visualize actin filaments, with a focus on key extracellular matrix (ECM) proteins and cell junction markers.

The cytoskeleton was labeled with rhodamine-phalloidin, appearing in purple [16], while cell nuclei were stained with DAPI (4′,6-diamidino-2-phenylindole), which emits a blue fluorescence [17]. These findings corroborate the formation of a well-structured spheroid, where cells are more closely associated, mimicking the characteristics of tumor spheroids.

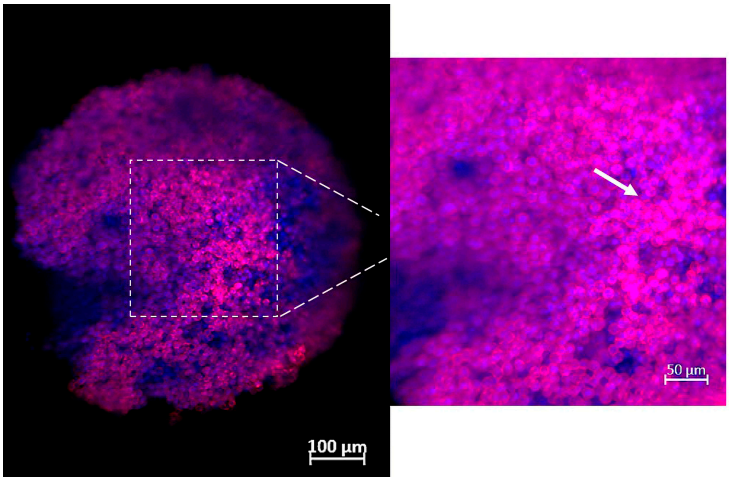

Figure 4. Immunofluorescence-labeled spheroid, blue and purple stains represent the cell nucleus and cytoskeleton markings (arrow), respectively.

Since the spheroid exhibited standard characteristics, the cytotoxicity of AuNPs@Ce6 was evaluated in microtumors using the MTT colorimetric assay. Viable cells with active metabolism convert the yellow MTT substrate into purple formazan crystals, producing an absorbance signal near 570 nm. According to the ISO 10993-5:2009 standard, substances that reduce metabolic activity to below 70% in in vitro assays are classified as cytotoxic [18]. Figure 5 shows the mean values obtained from two independent experiments conducted in triplicate under standardized conditions. Statistical analysis via one-way ANOVA followed by Tukey's post hoc test confirmed significant differences among the control, PDT, and dark cytotoxicity control groups (significance level of 0.05). The PDT group exhibited a cell viability of approximately 69%, indicating cytotoxicity, whereas the dark cytotoxicity control group (non-irradiated AuNPs@Ce6) maintained higher viability, confirming the absence of dark toxicity.

Figure 6 presents the results of the histological analysis of spheroids at the end of the cultivation period. These were sectioned into 5 µm thick sections and stained with hematoxylin-eosin, and the images were obtained microscopically with a 100x objective and immersion oil. Figure 6a shows the control samples in H&E staining, and Figure 6b corresponds to the micro-tumor treated with PDT associated with AuNPs@Ce6. The microscopic analysis of the slides revealed a purple-blue color in the cell nucleus due to its affinity with hematoxylin, while eosin, an acid dye, stained the cytoplasm in reddish tones, revealing structural details that enabled the observation of the interaction between cells and the extracellular matrix. It was also possible to observe significant differences between the experimental groups. The treated spheroids displayed swelling, pycnotic nuclei, eosinophilic cytoplasm, and karyorrhexis, which are hallmark features of cellular necrosis (see arrows in Figure 6b) [19], while the control group showed normal morphological features, including intact nuclei, defined cell borders, and uniform cytoplasmic staining.

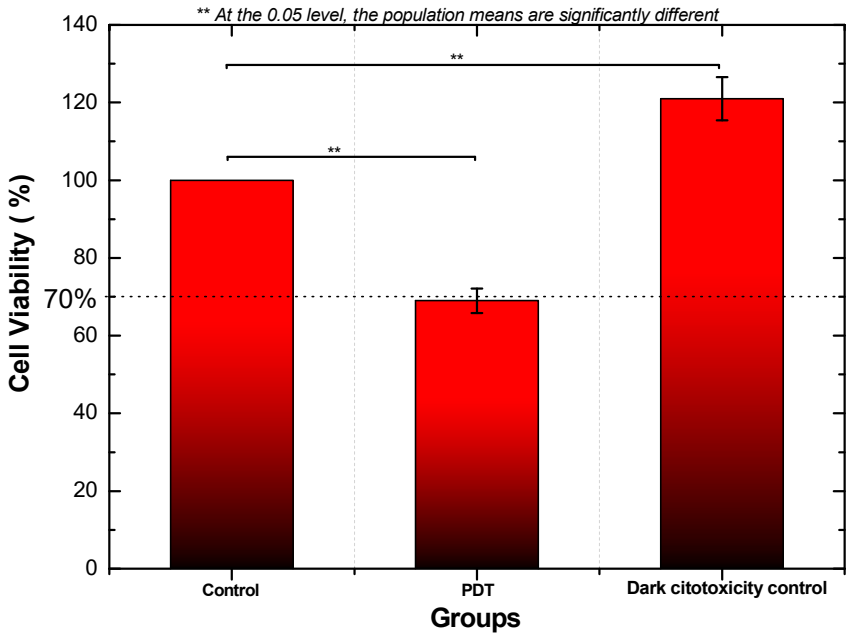

Figure 5. Results of the MTT assay for the following experimental groups of spheroids: control group (spheroids only), PDT group, and dark cytotoxicity control (AuNPs@Ce6 without irradiation). The standard deviations are represented by error bars, and ** indicates a statistically significant difference (significance level of 0.05) among the control, PDT, and dark cytotoxicity control groups, as determined by one-way ANOVA followed by Tukey's test.

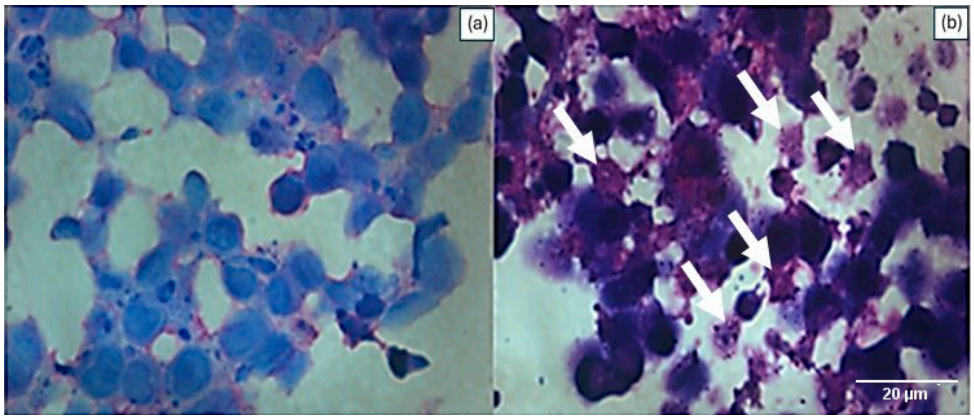

Figure 6. Histological analysis process: (**a**) control sample in H&E staining; (**b**) sample treated and irradiated with the AuNPs@Ce6. Arrows: necrotic cells. Both images were captured at the same magnification.

4. Discussion

The conjugation of Ce6 to AuNPs represents a promising strategy to enhance the efficacy of PDT [14]. Ce6 is a second-generation photosensitizer known for its strong absorption in the near-infrared region (650–700 nm), high singlet oxygen quantum yield, and relatively low dark toxicity [20]. However, its clinical potential is limited by poor water solubility, which could be enhanced by AuNP conjugation, improving Ce6 stability and cellular uptake, and enabling more efficient delivery [21]. To achieve Ce6 conjugation, carbodiimide coupling chemistry was employed using cysteamine as a linker, introducing a thiol group that forms a stable Au–S bond on the nanoparticle surface [22]. This modification is supported by Figure 1, where the LSPR band of AuNPs exhibits a redshift consistent with increased hydrodynamic diameter following functionalization. Additionally, the reduction in Zeta potential suggests the occurrence of conjugation, as it reflects enhanced

electrostatic stabilization within the system [15]. The UV-visible characterization showed that the AuNP@Ce6 spectrum is a combination of the absorption spectra of Ce6 and AuNPs, where the Soret band of AuNP@Ce6 has a blueshift of 11 nm and the Q band of Ce6 at 660 nm has a redshift of 8 nm.

According to Chen et al., nanoparticles with sizes around 22 nm show superior penetration in tumor spheroids because they can diffuse through both transcellular and paracellular pathways. Smaller particles (~15 nm) penetrate mainly through an energy-independent transcellular route, whereas larger ones (~60 nm) rely on an energy-dependent process, which limits their diffusion [23]. Thus, the AuNPs@Ce6 fall within the optimal size range for effective diffusion through microtumors.

Two-dimensional cell cultures have long been used in biomedical research due to their simplicity and cost-effectiveness [24]. However, they fail to reproduce the complex architecture and microenvironment of in vivo tissues [25]. In contrast, 3D cell culture models, such as spheroids, provide superior physiological relevance compared to conventional 2D cultures. They better replicate cell–cell and cell–matrix interactions and oxygen and nutrient gradients, closely resembling in vivo conditions [26,27]. Furthermore, 3D cultures exhibit more realistic drug diffusion and penetration profiles, improving the predictive value of therapeutic assays [28]. The formation of spheroids from cells of various cancer subtypes, including breast carcinomas, has driven research to explore the similarities between in vitro spheroids and in vivo models [29]. Despite their advantages, 3D systems require careful preparation and maintenance to prevent bacterial or fungal contamination.

In this study, 3D cell cultures were established using agarose micromolds with 800 µm and 1400 µm diameters, which enabled the formation of spheroids without cell adhesion to the walls of the micromolds. Over the cultivation period, a progressive growth of the spheroids was observed, which indicated a continuous cell proliferation, evidencing the efficacy of the culture method and viability of microtumor obtention [30]. The results reveal similar growth rates of $3.2 \pm 0.2\%$ and $3.9 \pm 0.4\%$ of the area covered per day for the 800 µm and 1400 µm mold diameters, respectively. For the 800 µm mold, spheroid growth initiated from the center and expanded toward the gelatin border, whereas for the 1400 µm mold, cell growth progressed from the border toward the center. However, a period of 40 days was necessary to achieve a compact spheroid suitable for handling during experimental procedures of PDT and cell viability. To analyze the structural proteins and ECM components of microtumors, the immunofluorescence technique was applied. The DAPI marker binds to the adenine–thymine regions of the DNA, exhibiting blue coloration marking the cell nucleus; rhodamine/phalloidin has an affinity for a fluorescent red-orange dye, tetramethylrhodamine (TRITC), highlighting the characteristics of the cytoskeleton. These results indicated that the cultured spheroids showed appropriate morphological and structural characteristics [31].

The MTT assay was employed to evaluate the cytotoxic effects of PDT associated with AuNPs@Ce6 on MDA-MB-468 spheroids. A non-irradiated (dark) control group was included to assess the inherent cytotoxicity of the AuNPs@Ce6. This assay measures mitochondrial dehydrogenase activity, which reduces MTT to insoluble formazan crystals, providing a direct indicator of cellular metabolic activity and viability. However, for 3D models, factors such as the number of spheroids, MTT concentration, and incubation time can significantly influence the amount of formazan generated. Therefore, standardization of the protocol was essential to ensure reliable and reproducible results [32]. PDT treatment reduced average mitochondrial activity to 69%, consistent with cytotoxicity thresholds [18]. Histological analysis confirmed necrosis features such as swelling, pycnotic nuclei, eosinophilic cytoplasm, and karyorrhexis [19]. In contrast, dark control samples exhibited an increase in mitochondrial activity (121% of control), indicating the absence of

dark toxicity, further confirmed by the normal histological morphology [33]. This slight elevation in metabolic activity may result from adaptive glycolytic or mitochondrial compensation typical of 3D spheroids, which exhibit enhanced ATP-linked respiration and non-aerobic ATP production under standard nutrient conditions [34].

Furthermore, the modulation of the incident light may dynamically influence the plasmonic response of the AuNPs@Ce6 system, potentially enhancing the energy transfer processes involved in photodynamic activation. Similar light-induced evolution of plasmonic properties has previously been demonstrated for AuNP-based systems under nanosecond pulsed irradiation [35], suggesting that tailored optical excitation conditions could further optimize the performance of the nanosystem during PDT.

The outcomes of this study gain particular relevance when compared with results from conventional 2D cell cultures. As reported in the literature, a single application of PDT using functionalized nanoparticles can lead to a near-complete reduction in cell viability under simplified in vitro conditions [36]. However, Dos Santos Jesus et al. [37], using a xenograft model of the MDA-MB-468 cell line, showed that although bifunctional nanoprobes conjugated with epidermal growth factor (EGF) and Ce6 induced significant tumor necrosis, a single PDT session was insufficient for complete tumor eradication. In this context, our results highlight the value of validating AuNPs@Ce6-mediated photodynamic therapy in 3D TNBC spheroids, which more accurately replicate tumor physiology and treatment response than 2D cultures. The 3D model produced reproducible cytotoxic and necrotic effects consistent with previous in vivo xenograft findings, even with variations in nanoparticle surface modification [38,39]. Although this proof-of-concept study evaluated only one nanoparticle concentration and a single TNBC cell line, these parameters were chosen to ensure experimental consistency. Overall, the use of 3D culture systems provides a physiologically relevant and ethically responsible intermediate model between 2D assays and animal studies, facilitating the refinement of nanostructured PDT parameters in accordance with the 3R principles—Replacement, Reduction, and Refinement [25].

5. Conclusions

AuNPs@Ce6 was successfully synthesized and shows promise as a strategy to enhance the efficacy of photodynamic therapy (PDT), addressing limitations related to Ce6's solubility, stability, and tumor targeting. The MTT assay and histological analyses were performed in 3D spheroid models using the MDA-MB-468 cell line. These experiments demonstrated that PDT with AuNPs@Ce6 effectively reduced cell viability and induced necrotic morphological changes. Additionally, the treatment showed biocompatibility in the non-irradiated control group. While these results are specific to the MDA-MB-468 TNBC model, they reinforce the potential of this approach for further investigation across additional TNBC subtypes. This study highlights the value of 3D cultures as a physiologically relevant and ethical alternative to animal testing, in line with the 3R principles of Replacement, Reduction, and Refinement. Future studies could explore different irradiation doses and nanoparticle concentrations to optimize therapeutic response.

Author Contributions: Investigation and writing—original draft, A.V.; formal analysis, G.C.G.; methodology C.P.S.; methodology, L.B.S.; formal analysis, V.L.M.M.; formal analysis S.K.S.; methodology, and supervision; writing—original draft preparation and supervision, L.R. All authors have read and agreed to the published version of the manuscript.

Funding: This research was funded by the CNPq [grant number 302158/2022-7] and FAPESP [2022/07411-5].

Institutional Review Board Statement: Not applicable.

Informed Consent Statement: Not applicable.

Data Availability Statement: The data that support the findings of this study are available from the corresponding author upon reasonable request.

Acknowledgments: Aveline Ventura would like to thank CAPES for the PhD scholarship.

Conflicts of Interest: The authors declare no conflicts of interest.

References

1. Roy, N.K.; Bordoloi, D.; Monisha, J.; Anip, A.; Padmavathi, G.; Kunnumakkara, A.B. Cancer—An Overview and Molecular Alterations in Cancer. In *Fusion Genes and Cancer*; World Scientific: Singapore, 2017; pp. 1–15. [CrossRef]
2. Tao, Z.; Shi, A.; Lu, C.; Song, T.; Zhang, Z.; Zhao, J. Breast Cancer: Epidemiology and Etiology. *Cell Biochem. Biophys.* **2015**, *72*, 333–338. [CrossRef]
3. Waks, A.G.; Winer, E.P. Breast Cancer Treatment. *JAMA* **2019**, *321*, 288. [CrossRef] [PubMed]
4. Gangi, A.; Chung, A.; Mirocha, J.; Liou, D.Z.; Leong, T.; Giuliano, A.E. Breast-conserving therapy for triple-negative breast cancer. *JAMA Surg.* **2014**, *149*, 252–258. [CrossRef] [PubMed]
5. Santonja, A.; Sánchez-Muñoz, A.; Lluch, A.; Chica-Parrado, M.R.; Albanell, J.; Chacón, J.I.; Antolín, S.; Jerez, J.M.; de la Haba, J.; de Luque, V.; et al. Triple negative breast cancer subtypes and pathologic complete response rate to neoadjuvant chemotherapy. *Oncotarget* **2018**, *9*, 26406. [CrossRef]
6. Abramson, V.G.; Lehmann, B.D.; Ballinger, T.J.; Pietenpol, J.A. Subtyping of triple-negative breast cancer: Implications for therapy. *Cancer* **2015**, *121*, 8–16. [CrossRef]
7. Wang, D.Y.; Jiang, Z.; Ben-David, Y.; Woodgett, J.R.; Zacksenhaus, E. Molecular stratification within triple-negative breast cancer subtypes. *Sci. Rep.* **2019**, *9*, 19107. [CrossRef]
8. Amraee, A.; Alamzadeh, Z.; Irajirad, R.; Sarikhani, A.; Ghaznavi, H.; Ghadiri Harvani, H.; Mahdavi, S.R.; Shirvalilou, S.; Khoei, S. Theranostic RGD@Fe_3O_4-Au/Gd NPs for the targeted radiotherapy and MR imaging of breast cancer. *Cancer Nanotechnol.* **2023**, *14*, 61. [CrossRef]
9. Vieira, P.; Jesus, V.; Cândido, M.A.; Pacheco-Soares, C.; Castilho, M.; Raniero, L. Specific nanomarkers fluorescence: In vitro analysis for EGFR overexpressed cells in triple-negative breast cancer and malignant glioblastoma. *Photodiagnosis Photodyn. Ther.* **2022**, *39*, 102997. [CrossRef]
10. Malatesti, N.; Harej, A.; Pavelić, S.K.; Lončarić, M.; Zorc, H.; Wittine, K.; Andjelkovic, U.; Josic, D. Synthesis, characterization and in vitro investigation of photodynamic activity of 5-(4-octadecanamidophenyl)-10, 15, 20-tris (N-methylpyridinium-3-yl) porphyrin trichloride on HeLa cells using low light fluence rate. *Photodiagnosis Photodyn. Ther.* **2016**, *15*, 115–126. [CrossRef]
11. Muguruma, M.; Teraoka, S.; Miyahara, K.; Ueda, A.; Asaoka, M.; Okazaki, M.; Kawate, T.; Kuroda, M.; Miyagi, Y.; Ishikawa, T. Differences in drug sensitivity between two-dimensional and three-dimensional culture systems in triple-negative breast cancer cell lines. *Biochem. Biophys. Res. Commun.* **2020**, *533*, 268–274. [CrossRef]
12. Turkevich, J.; Stevenson, P.C.; Hillier, J. A study of the nucleation and growth processes in the synthesis of colloidal gold. *Discuss. Faraday Soc.* **1951**, *11*, 55. [CrossRef]
13. Navarro, J.R.G.; Werts, M.H.V. Resonant light scattering spectroscopy of gold, silver and gold–silver alloy nanoparticles and optical detection in microfluidic channels. *Analyst* **2013**, *138*, 583–592. [CrossRef] [PubMed]
14. Vieira, L.; Castilho, M.L.; Ferreira, I.; Ferreira-Strixino, J.; Hewitt, K.C.; Raniero, L. Synthesis and characterization of gold nanostructured Chorin e6 for Photodynamic Therapy. *Photodiagnosis Photodyn. Ther.* **2017**, *18*, 6–11. [CrossRef] [PubMed]
15. Filho, O.O.C.; Cândido, M.A.; Ventura, A.; Morais, F.V.; Raniero, L. Nano-Enabled Colorimetric Assay for the Detection of *Paracoccidioides lutzii*: Advancing Diagnostics with Nanotechnology. *J. Nanotheranostics* **2024**, *5*, 75–83. [CrossRef]
16. McDonald, A.R.; Garbary, D.J.; Duckett, J.G. Rhodamine-Phalloidin Staining of F-Actin in Rhodophyta. *Biotech. Histochem.* **1993**, *68*, 91–98. [CrossRef]
17. Otto, F. Chapter 11 DAPI Staining of Fixed Cells for High-Resolution Flow Cytometry of Nuclear DNA. In *Methods in Cell Biology*; Elsevier: Amsterdam, The Netherlands, 1990; pp. 105–110. [CrossRef]
18. *ISO 10993-5:2009*; Biological Evaluation of Medical Devices—Part 5: Tests for In Vitro Cytotoxicity. International Organization for Standardization: Geneva, Switzerland, 2009. Available online: https://www.iso.org/standard/36406.html (accessed on 10 June 2024).
19. Bursch, W.; Taper, H.S.; Lauer, B.; Schulte-Hermann, R. Quantitative histological and histochemical studies on the occurrence and stages of controlled cell death (apoptosis) during regression of rat liver hyperplasia. *Virchows Arch. B Cell Pathol.* **1986**, *50*, 153–166. [CrossRef]
20. Hak, A.; Ali, M.S.; Sankaranarayanan, S.A.; Shinde, V.R.; Rengan, A.K. Chlorin e6: A Promising Photosensitizer in Photo-Based Cancer Nanomedicine. *ACS Appl. Bio Mater.* **2023**, *6*, 349–364. [CrossRef]

21. Li, Z.; Pan, W.; Shi, E.; Bai, L.; Liu, H.; Li, C.; Wang, Y.; Deng, J.; Wang, Y. A Multifunctional Nanosystem Based on Bacterial Cell-Penetrating Photosensitizer for Fighting Periodontitis via Combining Photodynamic and Antibiotic Therapies. *ACS Biomater. Sci. Eng.* **2021**, *7*, 772–786. [CrossRef]
22. Cândido, M.; Vieira, P.; Campos, A.; Soares, C.; Raniero, L. Gold-Coated Superparamagnetic Iron Oxide Nanoparticles Functionalized to EGF and Ce6 Complexes for Breast Cancer Diagnoses and Therapy. *Pharmaceutics* **2023**, *15*, 100. [CrossRef]
23. Chen, W.; Wang, W.; Xie, Z.; Centurion, F.; Sun, B.; Paterson, D.J.; Tsao, S.C.; Chu, D.; Shen, Y.; Mao, G.; et al. Size-Dependent Penetration of Nanoparticles in Tumor Spheroids: A Multidimensional and Quantitative Study of Transcellular and Paracellular Pathways. *Small* **2023**, *20*, e2304693. [CrossRef]
24. Ballav, S.; Jaywant Deshmukh, A.; Siddiqui, S.; Aich, J.; Basu, S. Two-Dimensional and Three-Dimensional Cell Culture and Their Applications. In *Cell Culture-Advanced Technology and Applications in Medical and Life Sciences*; IntechOpen: Rijeka, Croatia, 2022. [CrossRef]
25. Costa, E.C.; Moreira, A.F.; de Melo-Diogo, D.; Gaspar, V.M.; Carvalho, M.P.; Correia, I.J. 3D tumor spheroids: An overview on the tools and techniques used for their analysis. *Biotechnol. Adv.* **2016**, *34*, 1427–1441. [CrossRef] [PubMed]
26. Lin, R.Z.; Chang, H.Y. Recent advances in three-dimensional multicellular spheroid culture for biomedical research. *Biotechnol. J.* **2008**, *3*, 1172–1184. [CrossRef] [PubMed]
27. Tung, Y.C.; Hsiao, A.Y.; Allen, S.G.; Torisawa, Y.S.; Ho, M.; Takayama, S. High-throughput 3D spheroid culture and drug testing using a 384 hanging drop array. *Analyst* **2011**, *136*, 473–478. [CrossRef] [PubMed]
28. Russell, S.; Wojtkowiak, J.; Neilson, A.; Gillies, R.J. Metabolic profiling of healthy and cancerous tissues in 2D and 3D. *Sci. Rep.* **2017**, *7*, 15285. [CrossRef]
29. Langhans, S.A. Three-Dimensional in Vitro Cell Culture Models in Drug Discovery and Drug Repositioning. *Front. Pharmacol.* **2018**, *9*, 6. [CrossRef]
30. Boyer, C.J.; Ballard, D.H.; Barzegar, M.; Winny Yun, J.; Woerner, J.E.; Ghali, G.E.; Boktor, M.; Wang, Y.; Alexander, J.S. High-throughput scaffold-free microtissues through 3D printing. *3D Print. Med.* **2018**, *4*, 9. [CrossRef]
31. Dias-Netipanyj, M.F.; Cowden, K.; Sopchenski, L.; Cogo, S.C.; Elifio-Esposito, S.; Popat, K.C.; Soares, P. Effect of crystalline phases of titania nanotube arrays on adipose derived stem cell adhesion and proliferation. *Mater. Sci. Eng. C* **2019**, *103*, 109850. [CrossRef]
32. Buranaamnuay, K. The MTT assay application to measure the viability of spermatozoa: A variety of the assay protocols. *Open Vet. J.* **2021**, *11*, 251–269. [CrossRef]
33. Chan, J.K.C. The Wonderful Colors of the Hematoxylin–Eosin Stain in Diagnostic Surgical Pathology. *Int. J. Surg. Pathol.* **2014**, *22*, 12–32. [CrossRef]
34. Tidwell, T.R.; Røsland, G.V.; Tronstad, K.J.; Søreide, K.; Hagland, H.R. Metabolic flux analysis of 3D spheroids reveals significant differences in glucose metabolism from matched 2D cultures of colorectal cancer and pancreatic ductal adenocarcinoma cell lines. *Cancer Metab.* **2022**, *10*, 9. [CrossRef]
35. Martines-Arano, H.; García-Pérez, B.E.; Vidales-Hurtado, M.A.; Trejo-Valdez, M.; Hernández-Gómez, L.H.; Torres-Torres, C. Chaotic Signatures Exhibited by Plasmonic Effects in Au Nanoparticles with Cells. *Sensors* **2019**, *19*, 4728. [CrossRef] [PubMed]
36. Castilho, M.L.; Jesus Viviane, P.S.; Vieira, P.F.A.; Hewitt, K.C.; Raniero, L. Chlorin e6-EGF conjugated gold nanoparticles as a nanomedicine based therapeutic agent for triple negative breast cancer. *Photodiagnosis Photodyn. Ther.* **2021**, *33*, 102186. [CrossRef] [PubMed]
37. dos Santos Jesus, V.P.; Vieira, P.F.A.; Cintra, R.C.; Sant'Anna, L.B.; Zezell, D.M.; Castilho, M.L.; Raniero, L. Triple-negative breast cancer treatment in xenograft models by bifunctional nanoprobes combined to photodynamic therapy. *Photodiagnosis Photodyn. Ther.* **2022**, *38*, 102796. [CrossRef] [PubMed]
38. Urzì, O.; Gasparro, R.; Costanzo, E.; De Luca, A.; Giavaresi, G.; Fontana, S.; Alessandro, R. Three-Dimensional Cell Cultures: The Bridge between In Vitro and In Vivo Models. *Int. J. Mol. Sci.* **2023**, *24*, 12046. [CrossRef]
39. Gómez-Mercader, A.; Monzón-Atienza, L.; Montero, D.; Bravo, J.; Acosta, F. Fish Cell Spheroids, a Promising in Vitro Model to Mimic In Vivo Research: A Review. *Cells* **2024**, *13*, 1818. [CrossRef]